ChemComm

Check for updates

Stepwise construction of coordinative linkages and dynamic covalent linkages for a porous metal–organic framework†

Shuyin Peng, Yuqian Sun, Qingqing Li, Zhongwen Jiang, Yin Rao, Yichen Wu and Qiaowei Li ⓘ *

A cyclic trinuclear complex is synthesized from Ag^I and 1*H*-pyrazole-4-carbaldehyde. Reticulation of the complex with 1,3,5-tris(4-aminophenyl)benzene through Schiff-base reaction affords a porous FDM-72 framework. Amine choice is systematically investigated as it may initiate metal reduction. This study proposes a new route and its amine selection criterion to synthesize Ag-based frameworks.

Metal–organic frameworks (MOFs)[1] are a class of crystalline porous materials typically constructed from inorganic secondary building units (SBUs)[2] and organic linkers. Coordination linkages between metal ions and organic binding groups (carboxylates, azolates, *etc.*) are the main driving force that bring different constituents together and lock each other into well-defined frameworks. Recently, as an alternative route to synthesize MOFs, discrete coordination complexes with specific functional groups are being employed to react with organic units using dynamic covalent chemistry to achieve extended structures.[3] For example, [Ti$_6$O$_6$(COO)$_6$] clusters,[4] [Cr$_3$O(COO)$_6$] clusters,[5] [Zn$_4$(PO$_3$)$_4$] clusters,[6] and even polyoxometalates[7] with –NH$_2$/–CHO functionalities have been reticulated with organic aldehyde/amine through Schiff-base reaction. As a juncture of MOF and covalent organic framework (COF) chemistry,[8] the newly developed synthetic route involves the construction of both coordination linkages and dynamic covalent linkages in one framework.

In 2021, Li and our group reported the use of Cu$_3$(PyCA)$_3$ (HPyCA = 1*H*-pyrazole-4-carbaldehyde) as the basic modules for MOF construction through dynamic covalent chemistry.[9] The synthetic approaches have been practiced to build various reticular materials[9,10] targeting small molecule catalysis and

Department of Chemistry, Collaborative Innovation Center of Chemistry for Energy Materials, and Shanghai Key Laboratory of Molecular Catalysis and Innovative Materials, Fudan University, Shanghai 200433, P. R. China.
E-mail: qwli@fudan.edu.cn

photocatalytic CO$_2$ conversion applications, thanks to their abundant redox-active sites and periodic π–π conjugated system. However, applying the same stepwise synthetic strategy to frameworks based on other d^{10} metals, such as Ag, is less investigated. (i) For the coordination linkage construction, facile preparation and isolation of molecular Ag$_3$(PyCA)$_3$ has not been reported yet, and its crystal structure is desired for precise modelling of the corresponding extended structures. (ii) For the dynamic covalent linkage construction, Ag^I is more oxidative than Cu^I, and their compatibility with various amines featuring different reductive ability remains unexplored.

Herein, we report the successful synthesis of Ag$_3$(PyCA)$_3$ molecular single crystals through Ag–pyrazolate coordination. The triangular complex could serve as a 3-connected node when reacting with 1,3,5-tris(4-aminophenyl)benzene (TAPB) through Schiff-base reaction. With the help of stepwise coordination linkage and dynamic covalent linkage, Ag^I, PyCA, and TAPB are successfully reticulated into a two-dimensional (2D) honeycomb structure with layers packed in eclipsed fashion. Furthermore, the metal/amine compatibility investigation reveals that, while both *p*-phenylenediamine (PA) and TAPB are compatible with Cu$_3$(PyCA)$_3$, PA may reduce Ag$_3$(PyCA)$_3$ and complicate the framework construction. This study proposes not only a new route to synthesize Ag-based frameworks, but also a criterion for their building unit selection.

Through a solvothermal reaction of AgNO$_3$ and HPyCA in a mixture of *N,N*-diethylformamide (DEF), methanol, and H$_2$O at 100 °C for 12 h, Ag$_3$(PyCA)$_3$ crystals in needle shape are synthesized (Fig. 1, see the ESI,† for details). Single-crystal X-ray diffraction (SXRD) reveals that each Ag^I is linearly coordinated with two N from two (PyCA)$^-$, and three Ag^I form a trinuclear triangular complex with three (PyCA)$^-$. The complex with three –CHO groups is co-planar. In each unit cell, 16 Ag$_3$(PyCA)$_3$ molecules are arranged in a 4 × 4 fashion (Fig. S5a, ESI†). Slight rotation and tilting between neighbouring complexes results in a unit cell with long a and b cell parameters (Table S1, ESI†). π–π stacking between the complexes is evident, as the intermolecular distance is only 3.0 Å (Fig. S5b, ESI†).

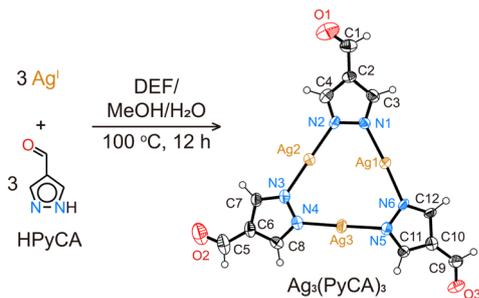**Fig. 1** Preparation of Ag₃(PyCA)₃ by coordinating Ag^I with HPyCA.

It should be noted that Ag^I is likely to be reduced to Ag during the complex synthesis, thus the obtained product is often a mixture of colorless Ag₃(PyCA)₃ crystals and black Ag particles (Fig. S1, ESI†). However, the Ag particles can be easily removed by dissolving Ag₃(PyCA)₃ in DMSO, followed by filtration and re-precipitation in methanol (Fig. S2, ESI†). Ag₃(PyCA)₃ is isostructural with the previously reported Cu₃(PyCA)₃·H₂O and Ag₃(Me₂PyBCA)₃ (Me₂PyBCA = 4-(3,5-dimethyl-pyrazol-4-yl)benzaldehyde).[9b,11] With three –CHO in the corners, the triangular Ag₃(PyCA)₃ could serve as a building unit to further build extended structures using dynamic covalent chemistry.

A crystalline material named FDM-72 (FDM = FuDan Materials) is obtained after heating Ag₃(PyCA)₃ in a TAPB solution in mesitylene, dioxane, and aqueous CH₃COOH at 50 °C for 72 h (Fig. 2a). Compared with the Fourier transform infrared (FT-IR) spectra of Ag₃(PyCA)₃ and TAPB, C=O stretching (1660 cm^{-1}) and N–H stretching (3424 and 3346 cm^{-1}) are not observed in FDM-72 (Fig. S3, ESI†). Furthermore, a new vibration at 1617 cm^{-1} in FDM-72 confirms the C=N bond formation, suggesting a Schiff-base reaction between Ag₃(PyCA)₃ and TAPB.

FDM-72 shows relatively strong low angle peaks (Fig. 3a) in powder X-ray diffraction (PXRD); however, determining its crystal structure using SXRD is not possible due to its small crystal size and inherent structural disorder. In addition, the PXRD with slight amorphization and weak diffraction at high angles is not enough for a reasonable Rietveld refinement.[10d,g] Since both Ag₃(PyCA)₃ and TAPB show C_3 symmetry, it is rational to build an FDM-72 structure model as 2D honeycomb
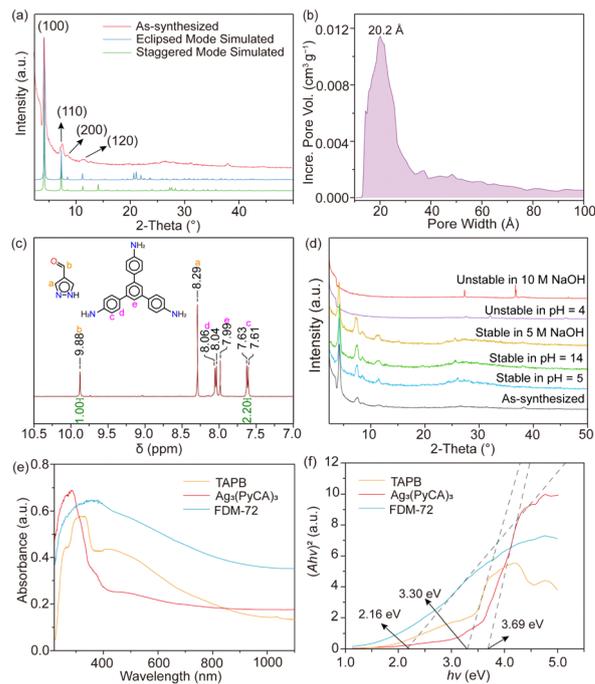

Fig. 3 (a) PXRD profiles of FDM-72 and simulation based on the eclipsed and staggered models. (b) Pore distribution profile of FDM-72 using the NLDFT adsorption model. (c) ¹H NMR of FDM-72 after DCl digestion and AgCl removal. (d) PXRD profiles of as-synthesized FDM-72 and FDM-72 after being soaked in various acid and base solutions for 7 days. (e) Diffuse reflectance UV-vis spectra of FDM-72, Ag₃(PyCA)₃, and TAPB. (f) The plots of $(Ah\nu)^2$ versus $h\nu$ for optical band gap calculation.

layers,[12] in which the tritopic Ag₃(PyCA)₃ and TAPB nodes are arranged alternatively within the layers (Fig. 2a). We modelled the two most possible stacking modes of the layers after applying geometry optimization of the constituents, and they are (i) eclipsed mode with AA packing of layers along the c axis in the $P\bar{6}$ space group, and (ii) the staggered mode with AB packing in space group $P6_3$ (Fig. 2b). Pawley refinement[13] is further performed based on the two structure models (see the ESI†). Specifically, for the eclipsed model, its unit cell parameters are refined to be a = 24.0661 Å, c = 4.2981 Å (Table S2 and Fig. S6, ESI†). On the other hand, for the staggered model,

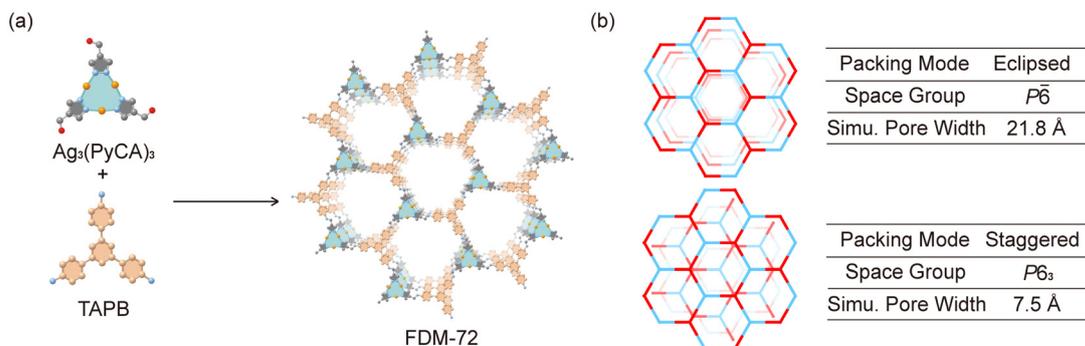**Fig. 2** (a) Synthesis of FDM-72 from Ag₃(PyCA)₃ and TAPB. In the Ag₃(PyCA)₃ unit: Ag, orange; C, grey; O, red; N, blue. In the TAPB unit: C, tan; N, blue. (b) Topology diagrams and parameters of the eclipsed and staggered stacking modes.

the parameters after refinement come to a = 23.7252 Å, c = 6.5299 Å (Table S3 and Fig. S7, ESI†). The experimental PXRD peaks at 2θ = 4.3, 7.5, 8.6 and 11.5° could be assigned to (100), (110), (200), and (120) planes in both models. However, the peaks at higher angles are relatively wide and weak (Fig. 3a), and unambiguous assignment to different planes in either model is not possible. Although the Pawley refinement shows marginally better agreement for the eclipsed model, determining the exact stacking mode of FDM-72 with high confidence needs additional experimental validation, such as its pore size distribution analysis.

The N_2 adsorption isotherm of FDM-72 is measured at 77 K after solvent exchange and sample activation. Moderate PXRD intensity still remains after the MOF is washed with N,N-dimethylformamide (DMF) (Fig. S8, ESI†), followed by supercritical CO_2 drying and 100 °C heating *in vacuo*. The adsorption isotherm can be characterized as a type IV isotherm featuring a clear hysteresis loop (Fig. S9, ESI†). The Brunauer–Emmett–Teller surface area (A_{BET}) of activated FDM-72 is calculated to be 395 m^2 g^{-1}, and its total pore volume is 0.448 cm^3 g^{-1}. We found that the experimental A_{BET} is much lower than the simulated values based on the eclipsed (2118 m^2 g^{-1}) or staggered model (1088 m^2 g^{-1}) using Zeo++,[14] indicating substantial inherent defects in FDM-72 and possible local structural collapse during the sample activation. Based on nonlocal density functional theory (NLDFT), FDM-72 features a wide pore size distribution between ~13 and 40 Å, with the peak centre at 20 Å (Fig. 3b). Pores larger than 40 Å are also evident, further confirming macroscopic defects in the framework.

Although the experimental A_{BET} is lower than the simulation, previous studies show that pore size is still a strong indicator of the layer packing mode.[9b,15] Theoretically, FDM-72 with eclipsed packing would have mesopores with 21.8 Å in diameter, while only micropores (d = 7.5 Å) exist in the staggered model. Comparing the experimental with the simulated pore size, we conclude that the layers in FDM-72 are stacked in eclipsed mode. Overall, the Ag_3-based FDM-72 is isostructural with the Cu_3-based JNM-1,[9a] suggesting that the Ag/Cu–pyrazolate coordination linkage doesn't interfere with the imine linkage formation, and a rational stepwise synthetic strategy could be developed for MOFs based on the trinuclear d^{10} metal complex.

To quantify the organic moieties in FDM-72, it is first digested by DCl and the obtained organic components are separated from AgCl precipitates for solution ^{1}H NMR measurement. Both the Ag–pyrazolate coordination linkage and the covalent imine linkage are dissociated during the digestion. Peak integration concludes that the molar ratio between PyCA and TAPB is 3.0 : 1.1 in FDM-72 (Fig. 3c), which is slightly deviated from the theoretical value (3 : 1). The observation suggests that PyCA vacancies are dominant in FDM-72.

Scanning electron microscopy (SEM) and energy-dispersive X-ray spectroscopy (EDX) confirm uniform element distribution in the crystalline material (Fig. S10, ESI†). X-Ray photoelectron spectroscopy (XPS) confirms that the oxidation state of Ag in FDM-72 is +1 (Fig. S11, ESI†). After the samples are kept in solutions with pH = 5–14, their PXRD patterns remain intact (Fig. 3d). Furthermore, FDM-72 still remains crystalline after it

is soaked in NaOH (5 M) for 7 days, confirming the high chemical stability of both the Ag–N coordination and C=N imine linkages. Further increasing the NaOH concentration to 10 M or lowering the acid pH value to 4 leads to the decomposition of the framework. The $Ag_3(PyCA)_3$ complex starts to decompose at 200 °C in thermogravimetric analysis (Fig. S12, ESI†). After the complexes are incorporated into the framework, FDM-72 is thermally stable up to 330 °C, indicating that the resulting scaffold is more resilient towards heat treatment after the formation of the imine linkage.

Highly conjugated π-orbital arrays in FDM-72 would enhance charge delocalization, resulting in small band gaps that contribute to high photoenergy conversion performances. In the UV-vis diffuse reflectance spectrum, the absorbance of the deep brown FDM-72 in the visible range is greatly signified compared with those of $Ag_3(PyCA)_3$ and TAPB, with the absorption peak at 400 nm (Fig. 3e). Using the Kubelka–Munk function, the optical band gap (E_g) of $Ag_3(PyCA)_3$ and TAPB is calculated to be 3.69 and 3.30 eV, respectively (Fig. 3f). After they are reticulated into the 2D framework, the optical band gap of FDM-72 is only 2.16 eV, confirming that the imine linkages build up a highly conjugated π–π system.[16] The electrochemical Mott–Schottky spectrum and valence band X-ray photoelectron spectrum (VB-XPS) of FDM-72 are further measured. Its conduction band position is estimated to be −0.38 V *versus* NHE (Fig. S13, ESI†), and the valence band edge is located at 1.73 eV (Fig. S14, ESI†). The calculated band gap (2.11 eV) based on the Mott–Schottky plots and the VB-XPS agrees with the optical band gap (2.16 eV).

Ag^I is known to be reduced easily even by a mild reducing agent, and a direct coordinative assembly between d^{10} metals (such as Ag^I and Au^I) and organic linkers often encounters unavoidable Ag or Au particles as by-products.[17] Separating the metal particles from the framework solids is not straightforward for most systems. In this work, we construct FDM-72 by connecting the coordination complex with tritopic amine through Schiff-base reaction. The molecular $Ag_3(PyCA)_3$ allows us to remove unwanted metal particles before the framework construction by simple dissolution and filtration, and thus the consequent FDM-72 is guaranteed to be phase pure. However, we are aware that different organic amines may have different redox potential, and the compatibility between the $Ag_3(PyCA)_3$ complex and different amines needs to be investigated to define the limit of the presented synthetic strategy.

We picked two isostructural trinuclear complexes based on two kinds of d^{10} metals (Cu^I and Ag^I) and two kinds of organic amines (TAPB and PA) for the compatibility study. $Cu_3(PyCA)_3$ is known to react with TAPB or PA to obtain JNM-1[9a] and FDM-71[9b] (Fig. 4a and b). No diffraction peak from Cu is observed in the product PXRD, confirming that neither amine could reduce Cu^I during the framework synthesis. Successful construction of FDM-72 proves that TAPB could not reduce Ag^I in $Ag_3(PyCA)_3$ to Ag (Fig. 4c). We now turn to the reaction between $Ag_3(PyCA)_3$ and PA to study the competition between Ag reduction and Schiff-base reaction in various MOF synthesis conditions.

Several attempts, such as mechanical grinding and solvothermal reactions in vials or Schlenk flasks, were applied to
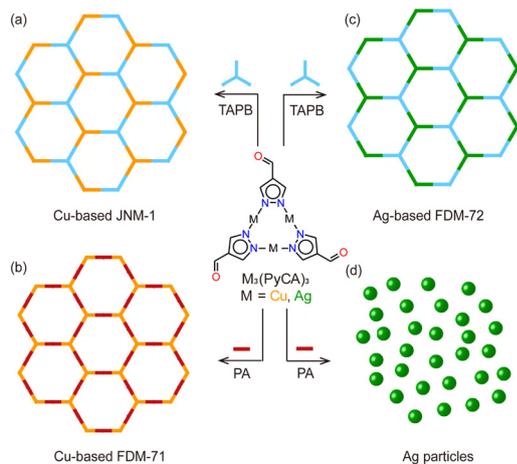
Fig. 4 Framework construction based on $M_3(PyCA)_3$ (M = Cu, Ag) and organic amines (TAPB and PA). (a) Cu-based JNM-1,[9a] (b) Cu-based FDM-71,[9b] and (c) Ag-based FDM-72 (this work) can be successfully obtained; however, (d) PA could reduce Ag^I in the $Ag_3(PyCA)_3$ complex and only Ag particles are formed.

the reaction of $Ag_3(PyCA)_3$ and PA. However, no crystalline framework was formed and only Ag particles were detected in PXRD (Fig. 4d and Fig. S4, ESI†). The reductive ability of PA is strong enough to reduce Ag^I in the complex and thus destroys the complex, while that of TAPB is weaker and does not lead to Ag precipitates. In the case of Cu^I-based $Cu_3(PyCA)_3$, using either PA or TAPB is safe for framework construction. Further cyclic voltammetry (CV) of PA and TAPB (0.054 M) reveals their oxidation potential at 0.58 and 1.12 V (*versus* SHE) (Fig. S15, ESI†). Given the reference that standard electrode potentials (E°) of $Ag^I(aq) + e^- \rightarrow Ag(s)$ and $Cu^I(aq) + e^- \rightarrow Cu(s)$ are 0.80 and 0.52 V, respectively, it is reasonable that the Ag^I and PA combination undergoes redox reaction, thus interrupting the framework construction. Overall, we propose that the coordination linkage formation, the dynamic covalent linkage formation, and the redox potential compatibility between the constituents all need to be considered for functional framework synthesis.

In summary, we report the synthesis and structure of the cyclic $Ag_3(PyCA)_3$ complex based on the coordination between three linear Ag^I and three PyCA ligands. The complex with three –CHO groups can serve as a 3-connected node for reticular structure. Furthermore, the dynamic covalent linkage between the complex and TAPB gives rise to FDM-72 with honeycomb layers stacked in an eclipsed fashion. FDM-72 shows 1D channels with 2.0 nm diameter, and an optical band gap of only 2.16 eV. The oxidative potential compatibility between the amine and the metal needs to be considered for the stepwise linkage construction, since the reductive amine may reduce the metal and thus interrupt the corresponding framework synthesis.

Conflicts of interest

There are no conflicts to declare.

Notes and references

1 (*a*) O. M. Yaghi, G. Li and H. Li, *Nature*, 1995, **378**, 703–706; (*b*) S. Kitagawa, R. Kitaura and S.-I. Noro, *Angew. Chem., Int. Ed.*, 2004, **43**, 2334–2375; (*c*) G. Férey, *Chem. Soc. Rev.*, 2008, **37**, 191–214; (*d*) J.-P. Zhang, Y.-B. Zhang, J.-B. Lin and X.-M. Chen, *Chem. Rev.*, 2012, **112**, 1001–1033; (*e*) H. Furukawa, K. E. Cordova, M. O'Keeffe and O. M. Yaghi, *Science*, 2013, **341**, 1230444; (*f*) S. Yuan, L. Feng, K. Wang, J. Pang, M. Bosch, C. Lollar, Y. Sun, J. Qin, X. Yang, P. Zhang, Q. Wang, L. Zou, Y. Zhang, L. Zhang, Y. Fang, J. Li and H.-C. Zhou, *Adv. Mater.*, 2018, **30**, 1704303.
2 M. J. Kalmutzki, N. Hanikel and O. M. Yaghi, *Sci. Adv.*, 2018, **4**, eaat9180.
3 (*a*) J. Dong, X. Han, Y. Liu, H. Li and Y. Cui, *Angew. Chem., Int. Ed.*, 2020, **59**, 13722–13733; (*b*) Y. Li, M. Karimi, Y.-N. Gong, N. Dai, V. Safarifard and H.-L. Jiang, *Matter*, 2021, **4**, 2230–2265.
4 (*a*) H. L. Nguyen, F. Gándara, H. Furukawa, T. L. H. Doan, K. E. Cordova and O. M. Yaghi, *J. Am. Chem. Soc.*, 2016, **138**, 4330–4333; (*b*) H. L. Nguyen, T. T. Vu, D. Le, T. L. H. Doan, V. Q. Nguyen and N. T. S. Phan, *ACS Catal.*, 2017, **7**, 338–342.
5 S. K. Elsaidi, M. H. Mohamed, J. S. Loring, B. P. McGrail and P. K. Thallapally, *ACS Appl. Mater. Interfaces*, 2016, **8**, 28424–28427.
6 R. Jangir, A. C. Kalita, D. Kaleeswaran, S. K. Gupta and R. Murugavel, *Chem. – Eur. J.*, 2018, **24**, 6178–6190.
7 (*a*) W. Xu, X. Pei, C. S. Diercks, H. Lyu, Z. Ji and O. M. Yaghi, *J. Am. Chem. Soc.*, 2019, **141**, 17522–17526; (*b*) R. Ma, N. Liu, T.-T. Lin, T. Zhao, S.-L. Huang and G.-Y. Yang, *J. Mater. Chem. A*, 2020, **8**, 8548–8553.
8 (*a*) A. P. Côté, A. I. Benin, N. W. Ockwig, M. O'Keeffe, A. J. Matzger and O. M. Yaghi, *Science*, 2005, **310**, 1166–1170; (*b*) C. S. Diercks and O. M. Yaghi, *Science*, 2017, **355**, eaal1585; (*c*) K. Geng, T. He, R. Liu, S. Dalapati, K. T. Tan, Z. Li, S. Tao, Y. Gong, Q. Jiang and D. Jiang, *Chem. Rev.*, 2020, **120**, 8814–8933.
9 (*a*) R.-J. Wei, H.-G. Zhou, Z.-Y. Zhang, G.-H. Ning and D. Li, *CCS Chem.*, 2021, **3**, 2045–2053; (*b*) X. Li, J. Wang, F. Xue, Y. Wu, H. Xu, T. Yi and Q. Li, *Angew. Chem., Int. Ed.*, 2021, **60**, 2534–2540.
10 (*a*) H.-G. Zhou, R.-Q. Xia, J. Zheng, D. Yuan, G.-H. Ning and D. Li, *Chem. Sci.*, 2021, **12**, 6280–6286; (*b*) J. Zhou, J. Li, L. Kan, L. Zhang, Q. Huang, Y. Yan, Y. Chen, J. Liu, S.-L. Li and Y.-Q. Lan, *Nat. Commun.*, 2022, **13**, 4681; (*c*) R.-J. Wei, P.-Y. You, H. Duan, M. Xie, R.-Q. Xia, X. Chen, X. Zhao, G.-H. Ning, A. I. Cooper and D. Li, *J. Am. Chem. Soc.*, 2022, **144**, 17487–17495; (*d*) X. Wang, X. Ding, Y. Jin, D. Qi, H. Wang, Y. Han, T. Wang and J. Jiang, *Angew. Chem., Int. Ed.*, 2023, **62**, e202302808; (*e*) J.-N. Chang, J.-W. Shi, Q. Li, S. Li, Y.-R. Wang, Y. Chen, F. Yu, S.-L. Li and Y.-Q. Lan, *Angew. Chem., Int. Ed.*, 2023, **62**, e202303606; (*f*) X.-C. Lin, Y.-M. Wang, X. Chen, P.-Y. You, K.-M. Mo, G.-H. Ning and D. Li, *Angew. Chem., Int. Ed.*, 2023, **62**, e202306497; (*g*) M. Zhang, P. Huang, J.-P. Liao, M.-Y. Yang, S.-B. Zhang, Y.-F. Liu, M. Lu, S.-L. Li, Y.-P. Cai and Y.-Q. Lan, *Angew. Chem., Int. Ed.*, 2023, **62**, e202311999; (*h*) J.-Y. Song, X. Chen, Y.-M. Wang, X. Luo, T.-E. Zhang, G.-H. Ning and D. Li, *Chem. – Asian J.*, 2023, **18**, e202300857.
11 H. Li, J. Luo, Z.-Y. Zhang, R.-J. Wei, M. Xie, Y.-L. Huang, G.-H. Ning and D. Li, *lnorg. Chem.*, 2022, **61**, 414–421.
12 R. Liu, K. T. Tan, Y. Gong, Y. Chen, Z. Li, S. Xie, T. He, Z. Lu, H. Yang and D. Jiang, *Chem. Soc. Rev.*, 2021, **50**, 120–242.
13 G. S. Pawley, *J. Appl. Crystallogr.*, 1981, **14**, 357–361.
14 T. F. Willems, C. H. Rycroft, M. Kazi, J. C. Meza and M. Haranczyk, *Microporous Mesoporous Mater.*, 2012, **149**, 134–141.
15 X. Wang, X. Han, J. Zhang, X. Wu, Y. Liu and Y. Cui, *J. Am. Chem. Soc.*, 2016, **138**, 12332–12335.
16 H. Wang, H. Wang, Z. Wang, L. Tang, G. Zeng, P. Xu, M. Chen, T. Xiong, C. Zhou, X. Li, D. Huang, Y. Zhu, Z. Wang and J. Tang, *Chem. Soc. Rev.*, 2020, **49**, 4135–4165.
17 R.-J. Wei, M. Xie, R.-Q. Xia, J. Chen, H.-J. Hu, G.-H. Ning and D. Li, *J. Am. Chem. Soc.*, 2023, **145**, 22720–22727.